Atmospheric Research 274 (2022) 106183

Contents lists available at ScienceDirect

Atmospheric Research

journal homepage: www.elsevier.com/locate/atmosres

Ability of the WRF-ARW and HARMONIE-AROME models to detect turbulence related to mountain waves over Central Iberia

J. Díaz-Fernández [a,*], P. Bolgiani [a], M. Sastre [a], D. Santos-Muñoz [b], F. Valero [a,c], J.I. Farrán [d], M. L. Martín [c,d]

[a] Department of Earth Physics and Astrophysics, Faculty of Physics, Complutense University of Madrid, Madrid, Spain
[b] Danmarks Meteorologiske Institut, Copenhaguen, Denmark
[c] Institute of Interdisciplinary Mathematics (IMI), Complutense University of Madrid, Madrid, Spain
[d] Department of Applied Mathematics, Faculty of Computer Engineering, University of Valladolid, Segovia, Spain

ARTICLE INFO

Keywords:
Turbulence
Eddy dissipation rate
WRF-ARW
HARMONIE-AROME
Mountain waves

ABSTRACT

Aircraft turbulence is one of the most dangerous meteorological phenomena that can affect aviation safety. This study is focused on the turbulence associated to mountain lee waves in the vicinity of Adolfo Suárez Madrid-Barajas airport (Spain). Sixty-eight mountain lee waves events are selected to simulate the turbulence with the Weather Research and Forecasting (WRF-ARW) and the HARMONIE-AROME numerical weather prediction models. To study and characterize the turbulence associated, the vertical wind speeds are selected as an important variable and the Eddy Dissipation Rate is estimated. Both models have properly simulated the turbulence and the clear air turbulence, obtaining higher values of turbulence intensity by WRF-ARW than HARMONIE-AROME in the mountain lee waves events. Finally, these results are used to enhance a mountain wave warning decision tree, including the turbulence warning which is validated through several turbulence reports.

1. Introduction

One of the most dangerous meteorological phenomena concerning aviation safety is the turbulence (NTSB, 2014; Gultepe et al., 2019; EASA, 2019). However, atmospheric turbulence must not be confused with the concept in aviation. FAA (2016) defined the turbulence as an irregular movement of an aircraft in flight caused by changes in the lift-up force created by an aircraft aerofoil. This lift-up force depends on the state of the atmosphere. Therefore, the turbulence is especially heavy when rapid changes in strong vertical winds (updrafts and downdrafts) are present in the atmosphere. This turbulence can be convective or mechanical (wind shear and orography). Here, a type of mechanical turbulence, the one associated with mountain lee waves, will be studied.

Mountain lee waves have been the subject of many investigations by the scientific community. The first studies on mountain lee waves, at high and low levels of the atmosphere, and their connection with turbulence were carried out by Kuettner (1939). Later, Lilly and Kennedy (1973), Clark and Peltier (1977) and Smith (1985) studied the process of mountain wave generation in major mountain ranges. Lane et al. (2009) demonstrated that 40% of the turbulence over Greenland was originated by mountain waves. Likewise, Kim and Chun (2011) evaluated the turbulence intensity, and they obtained that mountain lee waves triggered 20% of moderate to strong turbulence in South Korea.

Mountain lee waves are formed when a strong wind flow perpendicular to an orographic barrier climb up the mountain, promoting the air to ascend within a slightly stable layer. The waves can propagate vertically and/or horizontally (Broutman et al., 2001). These waves produce updrafts and downdrafts downwind and can generate associated lenticular clouds, which are formed in the updrafts and present as alternating bands of clouds. These lenticular clouds appear in the leeward of the orographic barrier when enough humidity exists (Geresdi and Rasmussen, 2005; Díaz-Fernández et al., 2021). These clouds can be indicative of the turbulence associated with mountain, but clear air turbulence (CAT) episodes can happen in cloud free regions (Sharman et al., 2012; Evans, 2014).

Diverse turbulence studies have used the vertical wind speed (Fernández-González et al., 2014; Bolgiani et al., 2018; Díaz-Fernández et al., 2020) and the Eddy Dissipation Rate (EDR) (Sarpkaya et al., 2001;

* Corresponding author.
E-mail address: javidi04@ucm.es (J. Díaz-Fernández).

https://doi.org/10.1016/j.atmosres.2022.106183
Received 13 December 2021; Received in revised form 4 April 2022; Accepted 5 April 2022
Available online 11 April 2022

Chan, 2010; Huang et al., 2019) as measurement for evaluating the turbulence. According to MacCready (1964), the EDR determine the quantity of energy lost by the viscous forces in a turbulent flow. The International Civil Aviation Organization (ICAO, 2001) provides turbulence categories (smooth to extreme) based on the EDR values for most aircraft. Moreover, direct estimates of EDR are available from some airlines (Sharman et al., 2014) and as an operational forecasting product called GTG (Graphical Turbulence Guidance) developed by the Aviation Weather Center (Sharman and Pearson, 2017). Here, turbulence associated with mountain lee waves is simulated using two numerical weather prediction models. The Weather Research and Forecasting Advanced Research (WRF-ARW, hereafter WRF; Skamarock and Klemp, 2008) and the HARMONIE-AROME (hereafter HARMONIE; Bengtsson et al., 2017). Moreover, a warning method to detect such turbulence is provided and evaluated.

2. Experimental design

2.1. Study area and datasets

The turbulence analysis related to mountain lee waves concerns the vicinity of Adolfo Suárez Madrid-Barajas airport (hereafter LEMD, as per the airport's International Civil Aviation Organization code). The airport elevation is 610 m above sea level (masl) and is located about 40 km south-east of the Guadarrama mountains. Moreover, the research area also covers three smaller airports: Cuatro Vientos (LECU), Getafe (LEGT) and Torrejón de Ardoz (LETO), all of them south-east of the Guadarrama mountain range. This range is placed in the centre of the Iberian Peninsula, with a length of 80 km and northeastern-southwestern orientation, The highest peak is Peñalara, 2428 masl. The mountain lee waves formation occur when the prevalent wind direction is north-northwest.

Following the methodology of Díaz-Fernández et al. (2021, 2022), 88 grid points are selected for turbulence detection in the leeward of the Guadarrama mountains. These follow the prevalent wind direction for these events and ensure at least one lee wave to be captured. The dataset used in the current paper corresponds to the one developed by Díaz-Fernández et al. (2021). Thus, 68 mountain lee waves events are simulated. These events belong to the winter season (November to March, when the mountain lee waves are more frequent in this study area) within the 2001–2010 period.

2.2. Numerical weather prediction models

The selected mountain lee waves events have been simulated using two high resolution numerical weather prediction models: HARMONIE and WRF using the same physics configurations, domains and model options as the study by Díaz-Fernández et al. (2022). According to Zovko-Rajak and Lane (2014), Trier and Sharman (2016), Sharman and Pearson (2017) and Díaz-Fernández et al. (2020), high-resolution simulations (below 3 km) are required to obtain acceptable forecasts of turbulence related to mountain lee waves due to the complexities of the physical processes involved.

The simulations performed with cycle 40 h1.1.1 of HARMONIE have a spatial resolution of 1 km and hourly temporal output. Each simulation is run in periods of 24 h, considering the first 6 h as spin-up. The HARMONIE configuration is a single domain with 65 hybrid sigma vertical levels and the physical parametrization used here is the default option defined by Bengtsson et al. (2017). Initial and boundary conditions are taken from the ERA5 reanalysis from European Centre for Medium-Range Weather Forecasts (ECMWF) global model with a temporal resolution of 1 h and 31 km for horizontal spatial resolution (Hersbach et al., 2020).

The simulations run with version 4.0.3 of WRF have a spatial resolution of 1 km, hourly temporal output, covering a period of 24 h with 6 h as spin-up time. The WRF configuration includes a two-ways strategy for four nested domains (27, 9, 3 and 1 km resolution), with 60 sigma levels. The microphysics parametrization used here is Thompson (Thompson et al., 2008) and the planetary boundary layer (PBL) is Yonsei University (Hong et al., 2006), as per Díaz-Fernández et al. (2020). Initial and boundary conditions for WRF are extracted from the National Centers for Environmental Prediction (NCEP) Climate Forecast System Reanalysis (CFSR), with a temporal resolution of 6 h and 0.5° for horizontal spatial resolution (Saha et al., 2010).

Different domain configurations were used for both models. As it is a spectral model and following its operational configuration a single domain was defined in HARMONIE. However, several domains with a grid nesting ratio of 3 were defined for WRF (finite-differences model). Moreover, different initial conditions have been used to select the optimum dataset for each model, as HARMONIE cannot run with the NCEP conditions and it has been proved that WRF performs worse when initiated with the ERA5 dataset (Bolgiani et al., 2020; Zhang et al., 2020). Although both models have different characteristics and configurations which can affect the results, they are run in the most similar way possible. It must be taken into account that the first-order YSU closure scheme used for WRF simulations directly expresses the eddy diffusivity (Troen and Mahrt, 1986). HARMONIE uses the RACMO Turbulence scheme, which has a first-order approximation too and avoids unnecessary vertical interpolations in the calculation of the turbulent fluxes (Bengtsson et al., 2017). This is relevant as we are dealing with microscale grid resolutions and variables' scales in *terra incognita* (Wyngaard, 2004). Mesoscale atmospheric models can compute the Turbulent Kinetic Energy (TKE) down to the grid resolution and then use parametrizations for subgrid computations. However, it's not clear that the energy dissipation behaviour is adequate for microscale. Rai et al. (2017) concludes that the threshold for the *terra incognita* in WRF is about 1.4 km, with very large variations in wind speed for resolutions below 0.8 km. Nonetheless, the turbulence we are aiming for in the present study is derived from mountain lee waves with wavelengths above 10 km, as per Díaz-Fernández et al. (2021, 2022) methodology. This requires steady and constant wind; thus, this issue should be a minor problem in the characterization performed.

3. Methodology

As specified above, 68 mountain lee waves episodes are selected using MSG-SEVIRI images between 2001 and 2010 from 08:00 to 17:00 UTC. The conditions required to consider a mountain lee wave event are those described by Díaz-Fernández et al. (2021): presence of at least three lenticular clouds bands southeast of the Guadarrama mountains, clouds brightness temperature between 260 and 275 K and wavelengths and transversal length greater than 15 km. The simulated EDRs are evaluated for characterization in 88 grid points leeward of the Guadarrama mountains. These calculations are performed at 2800 masl, following the mean altitude at which Bolgiani et al. (2018) and Díaz-Fernández et al. (2020) detected the highest liquid water content (LWC) values.

The Aviation Weather Center from NOAA (National Oceanic and Atmospheric Administration) issues operational forecasts of turbulence in the USA using the forecasting product GTG. This product establishes different degrees of turbulence based on the EDR calculation, which is used in this study. According to Sharman et al. (2014) the EDR ($m^{2/3}/s$) can be defined as

$$EDR = \varepsilon^{1/3} * 100 \quad (1)$$

where ε (m^2/s^3) is the eddy dissipation. Frech (2004) defined the eddy dissipation as

$$\varepsilon(z) = \frac{TKE(z)\ \frac{\partial U}{\partial z}}{C_{KP}^2} \quad (2)$$

where z is the altitude, TKE is the turbulent kinetic energy, U (u, v, w) is

the wind speed and C_{KP} is the Kolmogorov-Prandtl constant (Kramar and Kouznetsov, 2002) given as

$$C_{KP} = \left(\frac{TKE}{-\overline{u'w'}}\right)^{\frac{1}{2}} \quad (3)$$

being u' and w' the perturbations of the zonal and vertical wind components. According to Frech (2004), $C_{KP} \approx 2$ under neutral stability conditions.

Díaz-Fernández et al. (2021, 2022) proposed a methodology in which the percentiles for several atmospheric variables were obtained from the WRF and HARMONIE simulations and used to develop decision trees to warn about the presence of three different phenomena: mountain lee waves (considering wind direction and speed on the windward of the mountain range, and atmospheric stability over Guadarrama mountains), lenticular clouds (considering LWC) and icing (considering temperature) in the leeward of the mountains. From the Díaz-Fernández et al. (2021, 2022) methodology, in the current study a new decision tree is developed, including turbulence information from EDR values. Díaz-Fernández et al. (2021, 2022) considered different percentiles to characterize the mountain lee waves episodes, choosing the most consistent ones, in terms of meteorology, to reduce the impact of the arbitrary election. Finally, the 10th and 90th percentiles were selected as thresholds, because according to the mountain lee waves climatology and observations, these values were the most suitable ones. In the current study, fixed percentiles are again used since they turn out to be more suitable and easily transferable to other regions (Shevchenko et al., 2013). We keep working with the P10 and P90 to divide the decision tree prior to the turbulence/EDR warning, i.e., those values are chosen in wind direction and speed and static stability thresholds. Following Díaz-Fernández et al. (2022) methodology, several EDR percentiles are also calculated and studied (not shown), choosing the EDR 10th percentile (P10) as the most suitable one. Thus, P10 is an appropriate threshold for the last step of turbulence warning.

4. Results and discussion

This section is structured as follows: first, a case study is presented where vertical wind speed and the EDR simulated by WRF and HARMONIE can be observed in the study area. Then, the EDR probability density function and the related percentiles for the total events are shown. All the results presented in this section are calculated and represented for the 1 km resolution domain for both models.

4.1. Case study

To show the ability of both models to reproduce the turbulence associated with mountain lee waves events, a case study is presented. This will give the reader a clear idea of how the models represent the phenomenon, which will ease further analysis. The mountain lee wave case selected, corresponding to 06 November 2009 at 13:00 UTC, was produced by northwestern winds over the Guadarrama mountains, promoted by a positive North Atlantic Oscillation, which was due to a

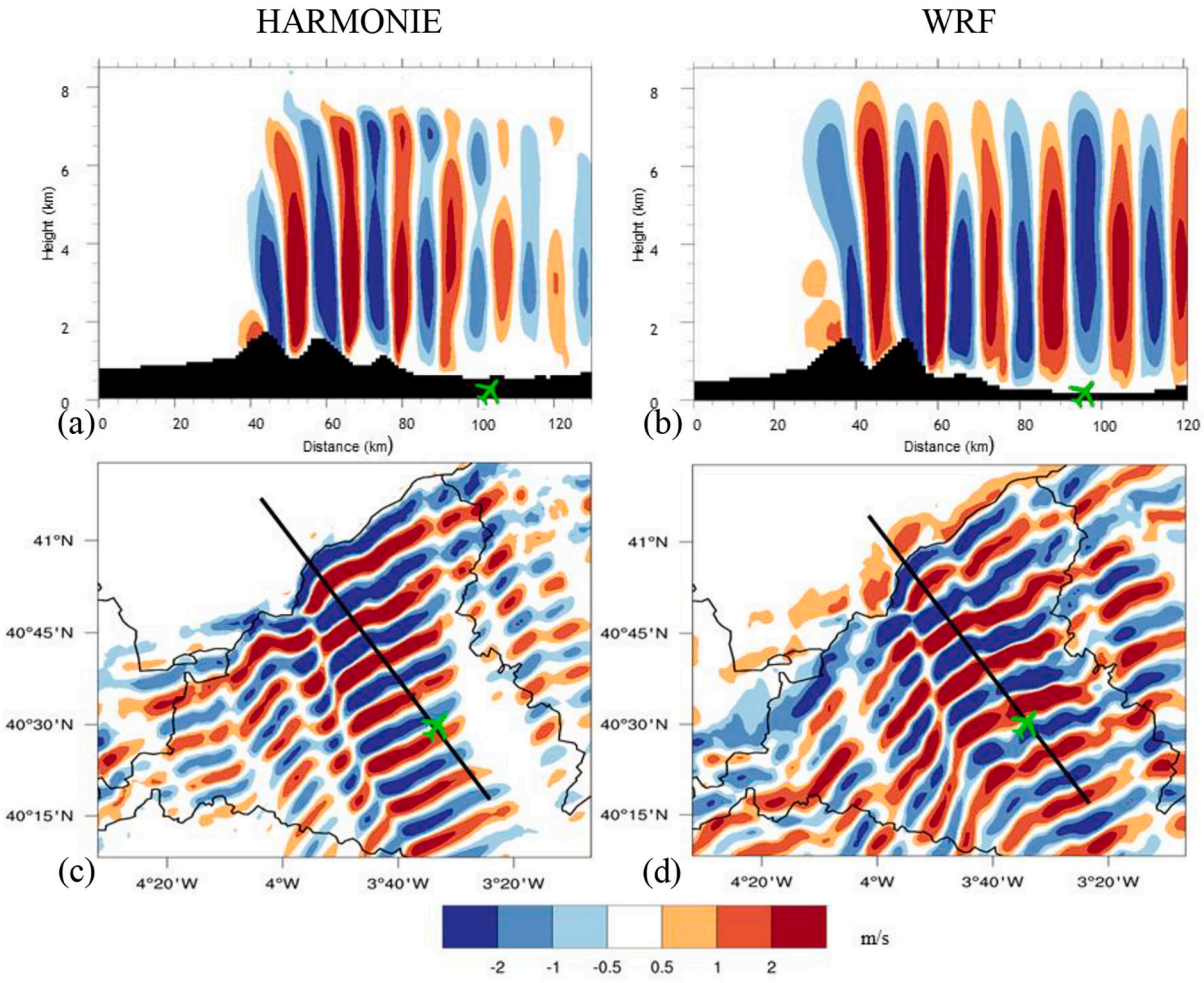

Fig. 1. Vertical wind speed (m/s) on 06 November 2009 at 13:00 UTC. (a) HARMONIE Cross section. (b) WRF Cross section. (c) HARMONIE at 2800 masl. (d) WRF at 2800 masl. Aircraft symbols correspond to LEMD location and the black line indicates the cross section used.

strong Icelandic Low and a strong Azores High.

A vertical wind speed cross section (Fig. 1a, b) and horizontal plot at 2800 masl (Fig. 1c, d) are displayed for both models over the study area. Several alternating downdrafts/updrafts bands can be observed leeward of the Guadarrama mountains range, reaching vertical wind speeds above ±2 m/s and an altitude of 7 km approximately. HARMONIE and WRF results for vertical wind speed are very similar. Only a few differences can be observed at the east of the LEMD airport where HARMONIE shows a blank area with no wave propagation while WRF displays a disrupted but still propagating wave (Fig. 1c, d). In the cross section, it can be seen that WRF simulated lee waves reach farther south than those simulated by HARMONIE. Alternating downdrafts and updrafts up to a height of 7 km were also observed in other mountain lee waves related studies (Bolgiani et al., 2018; Fernández-González et al., 2019; Díaz-Fernández et al., 2020). Moreover, according to Bolgiani et al. (2018) and Ikeda et al. (2007) these vertical wind speed values (> ± 2 m/s) can lead to moderate to strong turbulence for aircraft flying in the area.

TKE and EDR results for the case study analysed are depicted in Fig. 2 and Fig. 3 respectively. As the EDR depends on TKE (see Eq. (2); Frech, 2004), the results can be compared. TKE results (Fig. 2) show the highest TKE values in leeward for both HARMONIE and WRF models. However, TKE values are noteworthy higher for WRF than for HARMONIE. The cross sections (Fig. 2a and b) of both models show values higher than 5 m^2/s^2 leeward with HARMONIE TKE constraint to the lowest 3 km, while WRF TKE shows considerable values up to 8 km. The HARMONIE TKE values could be considered unrealistic since there are values close to 0 m^2/s^2 above the PBL, which is highly improbable in episodes of mountain lee waves (Večenaj et al., 2011; Parker and Lane, 2013).

As expected per the previous results, the maximum EDR simulated by HARMONIE (Fig. 3a) and WRF (Fig. 3b) are located leeward of the Guadarrama mountains. However, the highest values produced by HARMONIE range from 30 to 35 $m^{2/3}/s$ while the ones by WRF reach up to 45 $m^{2/3}/s$. According to Sharman et al. (2006), the turbulence expected as per the standard turbulence categories would be moderate for HARMONIE and severe for WRF in a light aircraft case (< 7000 kg). For medium aircraft (between 7000 and 136,000 kg), the turbulence would be moderate for both models. The location of the maximum values is very similar for both models, although at different altitudes. While for HARMONIE the maximum is located leeward of the second peak at 2 km of altitude, the WRF simulated this maximum just behind the second peak at an altitude of 1 km as it can be seen in Fig. 2a, b. On the other hand, HARMONIE produces no EDR values higher than 5 $m^{2/3}/s$ above 3 km of altitude, while the WRF EDR values reach up to 25 $m^{2/3}/s$ in the mentioned layer.

The horizontal distribution of EDRs for the two models shows notable differences. The mountain lee waves can be clearly identified in the HARMONIE at 2800 masl (Fig. 3c), while in the WRF this is not possible (Fig. 3d). HARMONIE produces a clear and distinct pattern, limiting the presence of turbulence to those areas directly affected by orography or the mountain wave. On the other hand, WRF generates turbulence all across the domain, with no organized pattern and higher values than those produced by HARMONIE. This follows the line of the aforementioned vertical results, by which WRF tends to generate more

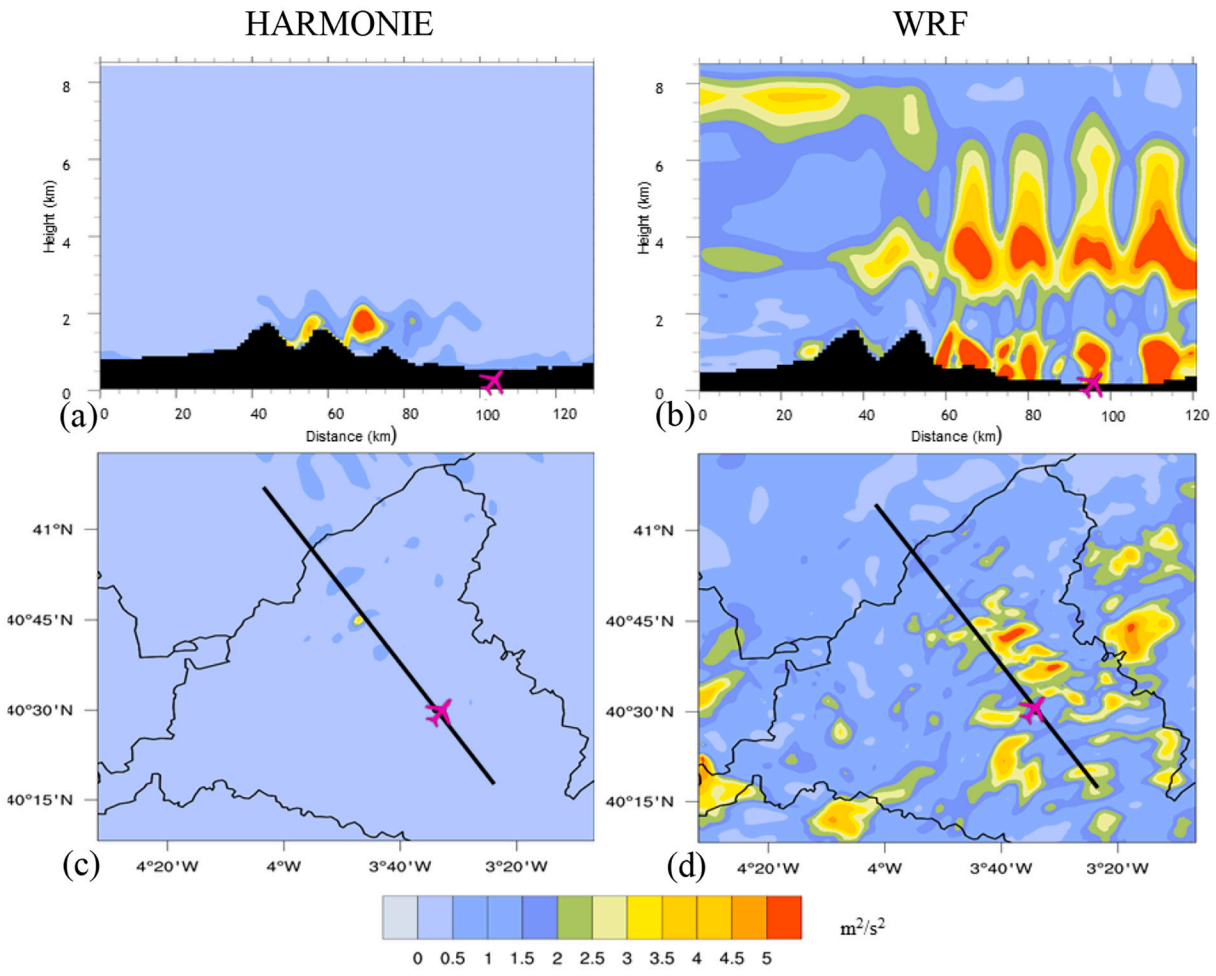

Fig. 2. TKE (m^2/s^2) on 06 November 2009 at 13:00 UTC. (a) HARMONIE Cross section. (b) WRF Cross section. (c) HARMONIE at 2800 masl. (d) WRF at 2800 masl. Aircraft symbols correspond to LEMD location and the black line indicates the cross section used.

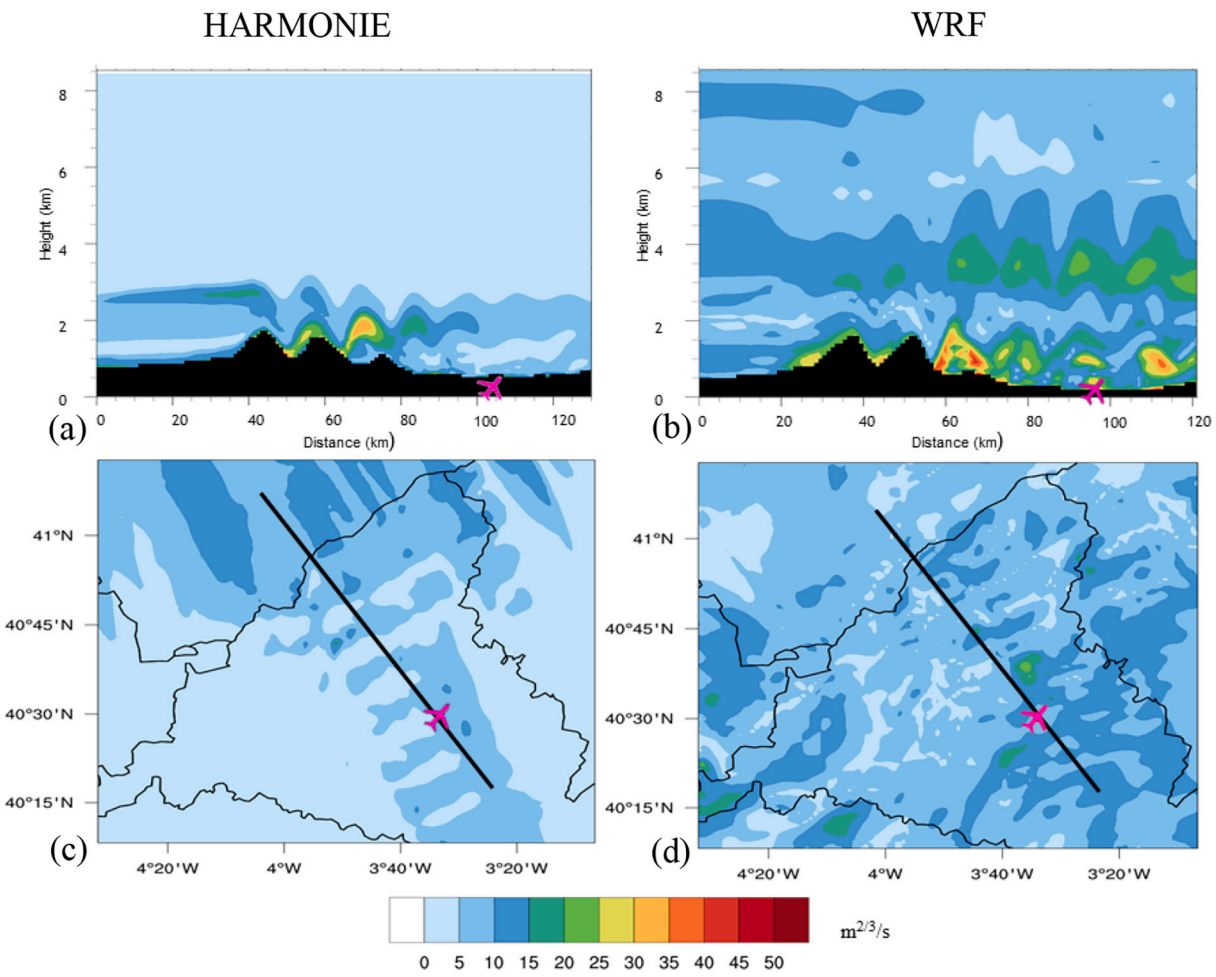

Fig. 3. EDR ($m^{2/3}/s$) on 06 November 2009 at 13:00 UTC. (a) HARMONIE Cross section. (b) WRF Cross section. (c) HARMONIE at 2800 masl. (d) WRF at 2800 masl. Aircraft symbols correspond to LEMD location and the black line indicates the cross section used.

turbulent flows in the domain.

Comparing Figs. 2 (TKE) and 3 (EDR) it can be observed that areas with higher TKE values for WRF match to higher EDR values simulated by this model. On the contrary, zones with small TKE values for HARMONIE do not show agreement in the EDR pattern. Therefore, the EDR major differences from both models cannot be singly explained by the

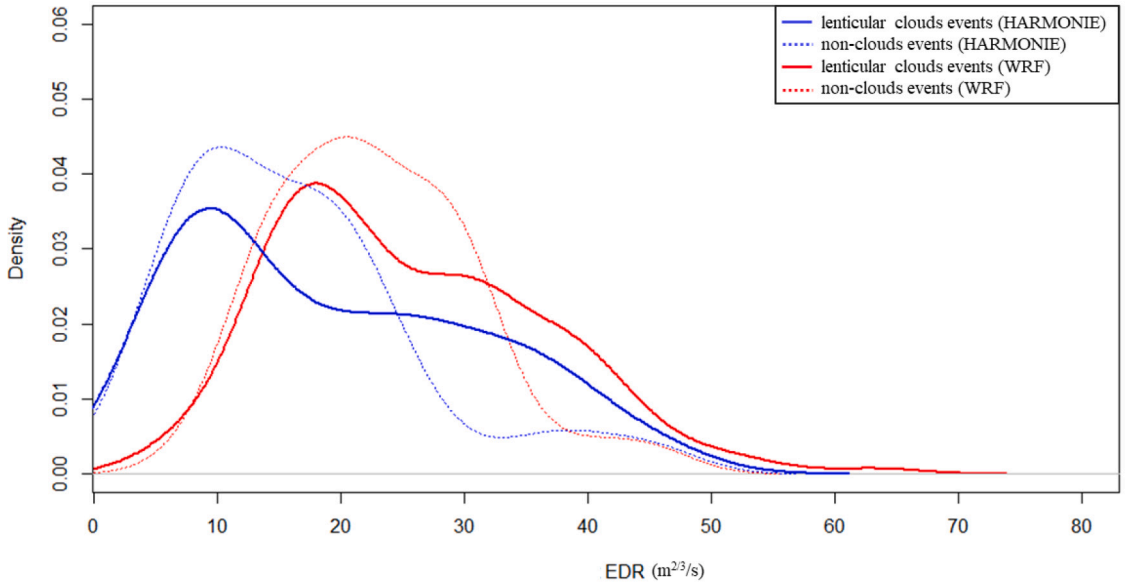

Fig. 4. Probability density functions of maximum EDR ($m^{2/3}/s$) on the leeward for HARMONIE and WRF models for lenticular clouds and non-clouds events.

TKE. Taking the Eq. (2) into account, the differences between the EDR simulations could be associated to the wind shear. In fact, wind speeds in vertical profiles ($\frac{\partial U}{\partial z}$, *wind shear*) are calculated for the selected mountain lee waves events (not shown), obtaining an overestimation for the lower atmospheric levels (up to 3 km) around 5 m/s in the WRF wind speed values in comparison with the HARMONIE ones. Moreover, this WRF overestimation agrees with the results by Díaz-Fernández et al. (2022) on mountain lee waves over the Guadarrama mountains. Therefore, it seems that the wind shear plays an important role in the turbulence diagnosis.

4.2. EDR characterization

Fig. 4 depicts the probability density functions of the simulated EDR maxima in each time step for the 88 selected grid points. Notable differences can be seen between the models, also between cloud events (inferred presence of strong mountain lee waves) and non-cloud events. For both models, the turbulence intensity can reach higher values when there is presence of lenticular clouds. This can clearly be seen at an EDR equal to 30 $m^{2/3}/s$ for HARMONIE, and equal to 40 $m^{2/3}/s$ for WRF, where the non-cloud events show almost no density for turbulence while the cloud-events still present a probability for it. Nevertheless, more events of light turbulence are obtained without the presence of clouds. Considering the vertical currents in each mountain lee wave event (as in Fig. 1c, d), the updrafts/downdrafts appear a few hours before that lenticular clouds bands and disappear few hours later. However, the vertical wind speed values are greater when lenticular clouds appear, which explains this difference in the probability density function.

It is also noteworthy that the EDR modal value is greater for WRF than HARMONIE, clearly seen in the lateral shift to higher EDR values generated by the WRF curves, which concurs with the results presented in the case study. The EDR percentiles results also show notable differences. The P10 for WRF (HARMONIE) is 14 (6) $m^{2/3}/s$, P25 is 17 (10) $m^{2/3}/s$ P50 is 23 (18) $m^{2/3}/s$, P75 is 33 (29) $m^{2/3}/s$ and P90 is 40 (37) $m^{2/3}/s$. This is in line with the larger differences between the model's curves at low EDR values. Following the turbulence categories defined by Sharman et al. (2006) for medium aircraft, light turbulence can be considered with EDR between 15 and 20 $m^{2/3}/s$, moderate between 20 and 44 $m^{2/3}/s$, severe 44 to 79 $m^{2/3}/s$ and extreme with EDR $\geq$ 79 $m^{2/3}/s$. It is remarkable that the EDR-P10 value for the WRF characterization matches with the light turbulence threshold defined by these authors.

As per the results presented here, the turbulence category is light in 22% of mountain lee waves events with lenticular clouds associated, moderate in 59% and severe in 5% for WRF results. For HARMONIE, 11% corresponds to light, 43% to moderate and 2% to severe turbulence. In none of the events the extreme turbulence reached. Therefore, it can be concluded that the 86% of mountain lee waves events simulated by WRF generate turbulence associated. This percentage decreases to 55% in the case of HARMONIE model. This HARMONIE percentage is closer to the Kim and Chun (2011) values, who demonstrated that mountain lee waves caused 20% of moderate to strong turbulence in South Korea.

Once the EDR percentiles from WRF and HARMONIE are obtained, the decision trees developed by Díaz-Fernández et al. (2021, 2022) are recalculated, considering P10 as thresholds (EDR-P10 = 14 $m^{2/3}/s$ for WRF and EDR-P10 = 6 $m^{2/3}/s$ for HARMONIE) in a new warning branch after the static stability. This means that, if the stability values are met, the EDR is considered and when the thresholds are reached, a turbulence warning would be issued (Fig. 5).

The EDR warning developed is validated using a dataset with recorded turbulence episodes from 2000 to 2021. The turbulence data base consists of 10 events, with 7 events associated to turbulence reports related to mountain lee wave events in the study area, and the remainder are random days. The turbulence reports are extracted for the pilot reports (PIREPs, https://mesonet.agron.iastate.edu/request/gis/pireps.php), the Spanish commission for the investigation of civil aviation accidents and incidents reports (CIAIAC, https://www.mitma.gob.es/organos-colegiados/ciaiac/investigacion) and a turbulent and icing report occurred on 28 February 2017 and studied by Bolgiani et al. (2018). As in Díaz-Fernández et al. (2021, 2022) studies, the EDR warning is validated using a contingency table for dichotomous verification of WRF and HARMONIE forecast (24 to 30 h before the event). Subsequently, the False Alarm Ratio (FAR), Probability of Detection (POD), frequency BIAS and Percent Correct (PC) skill scores are calculated to assess the EDR warning ability.

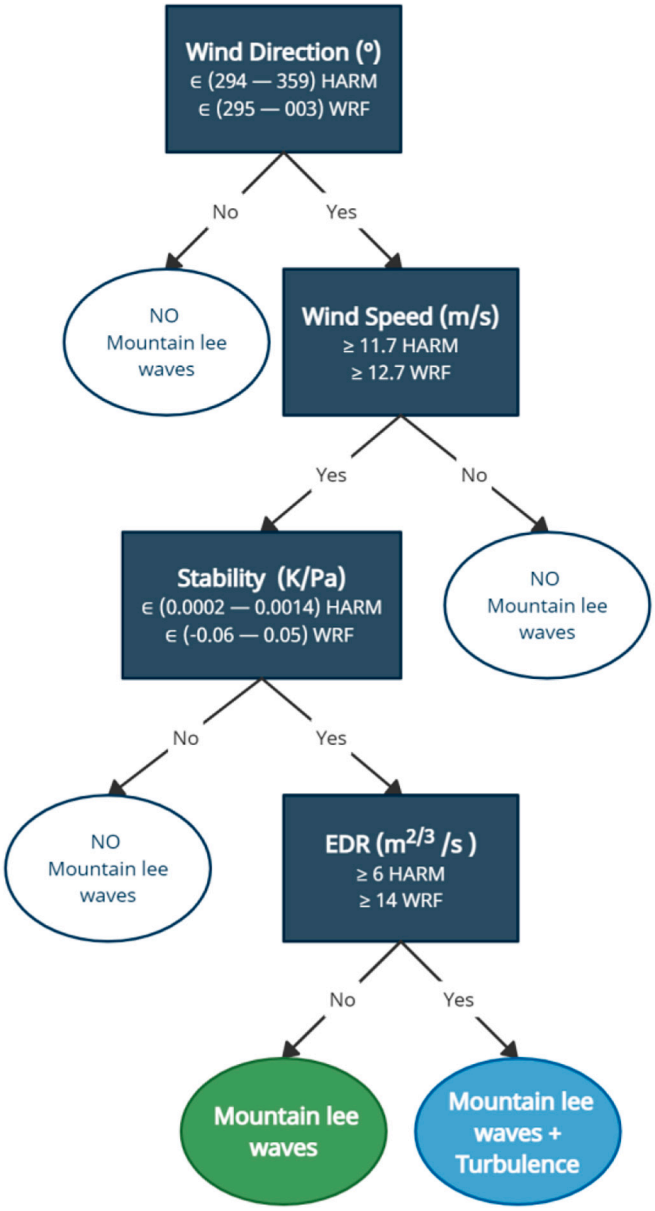

Fig. 5. Decision tree created for HARMONIE (HARM in the rectangles) and WRF highlighting the 10th and 90th percentiles used as thresholds.

The skill scores results show notable differences between both models, except for the FAR (equal 0 in both models). POD and BIAS for WRF (HARMONIE) are 0.83 (0.58) and PC is 0.80 (0.65). Therefore, the EDR warning for WRF obtains better results than for the HARMONIE. If the results of the EDR warning are compared to those of the three warnings developed by Díaz-Fernández et al. (2022) related to mountain wave and icing events, it can be noted that WRF simulates more accurately mountain lee waves and EDR. On the other hand, HARMONIE obtained better skill scores for the icing warning associated with

mountain lee waves. Therefore, it could be concluded that WRF performs better simulations related to mechanical variables (wind and TKE) while HARMONIE seems to capture the thermodynamics variables better (temperature).

Finally, comparing the WRF and HARMONIE behaviour in turbulence warnings associated with mountain lee waves with the case study presented before, it is observed that both models simulate the variables involved in turbulence (TKE and EDR) in a different way. This is also consistent with the skill score results. Besides, vertical wind speed does not seem to be a good indicator to study the turbulence associated with mountain lee waves, since the results are very similar for both models. However, when the EDR is considered, important differences are displayed. Therefore, the turbulence study seems more accurate if the EDR is considered and the EDR-P10 value is selected as threshold in the decision tree, being consistent with the case study.

5. Conclusions

A characterization of turbulence associated to mountain lee waves in the Guadarrama mountain range, near to LEMD airport, was carried out using WRF and HARMONIE models. The vertical wind speed and the EDR have been successfully evaluated to know the turbulence intensity associated to these events. Also, the results show the ability of the models to detect CAT when lenticular clouds are not present. Moreover, based on probability density functions of the maximum EDR, the highest values of EDR were obtained when lenticular cloud bands associated to mountain lee waves are diagnosed in the leeward of the mountain range.

The EDR characterization shows higher turbulence values for WRF compared to HARMONIE. Turbulence was simulated in the 86% of the mountain lee waves events with the WRF model and in the 55% from HARMONIE. This may be related to a wind speed difference between the models, about 5 m/s less for HARMONIE.

Concerning TKE and EDR results, the importance of both parameters has been evaluated. While TKE is not a single determining factor to evaluate the turbulence associated with mountain lee waves, the wind shear reveals as an important role in the turbulent events, rendering EDR a better forecasting variable.

Considering the EDR-P10 as threshold, a new branch in the decision tree, previously developed in Díaz-Fernández et al. (2021, 2022), was added to establish a warning. The turbulence warning associated with mountain lee waves events has been validated against turbulence reports of pilot reports and accidents and incidents reports, showing that EDR skill scores for the WRF model seem to be better than those obtained with HARMONIE.

As the Aviation Weather Center is currently doing in the USA, the EDR could be implemented as an operational tool to forecast the turbulence over the Iberian Peninsula. Moreover, it should also be added in the decision trees used to develop the warnings due to the better results obtained.

CRediT authorship contribution statement

J. Díaz-Fernández: Methodology, Software, Validation, Writing – review & editing, Data curation, Formal analysis. **P. Bolgiani:** Methodology, Software, Validation, Writing – review & editing, Data curation. **M. Sastre:** Methodology, Supervision, Investigation. **D. Santos-Muñoz:** Methodology, Software, Validation, Supervision. **F. Valero:** Funding acquisition, Resources, Investigation. **J.I. Farrán:** Software. **M. L. Martín:** Methodology, Validation, Writing – review & editing, Supervision, Funding acquisition, Resources, Investigation.

Declaration of Competing Interest

The authors declare that they have no known competing financial interests or personal relationships that could have appeared to influence the work reported in this paper.

Acknowledgments

This work was partially supported by research projects PID2019-105306RB-I00 (IBERCANES project), CGL2016-78702-C2-1-R and CGL2016-78702-C2-2-R (SAFEFLIGHT project), FEI-EU-17-16 and SPESMART AND SPESVALE (ECMWF Special Projects). J. Díaz-Fernández acknowledges the grant supported by the Ministerio de Ciencia, Innovación y Universidades (FPI program BES-2017-080025).

References

Bengtsson, L., Andrae, U., Aspelien, T., Batrak, Y., Calvo, J., de Rooy, W., Gleeson, E., Hansen-Sass, B., Homleid, M., Hortal, M., Ivarsson, K.-I., Lenderink, G., Niemelä, S., Nielsen, K.P., Onvlee, J., Rontu, L., Samuelsson, P., Muñoz, D.S., Subias, A., Køltzow, M.Ø., 2017. The HARMONIE– AROME Model Configuration in the ALADIN–HIRLAM NWP System. Mon. Weather Rev. 145 (5), 1919–1935. https://doi.org/10.1175/MWR-D-16-0417.1.1.

Bolgiani, P., Fernández-González, S., Martin, M.L., Valero, F., Merino, A., García-Ortega, E., Sánchez, J.L., 2018. Analysis and numerical simulation of an aircraft icing episode near Adolfo Suárez Madrid-Barajas International Airport. Atmos. Res. 200, 60–69. https://doi.org/10.1016/j.atmosres.2017.10.001.

Bolgiani, Pedro, Santos-Muñoz, Daniel, Fernández-González, Sergio, Sastre, Mariano, Valero, Francisco, Martín, María Luisa, 2020. Microburst Detection With the WRF Model: Effective Resolution and Forecasting Indices. J. Geophys. Res.: Atmos. 125 https://doi.org/10.1029/2020JD032883. In press.

Broutman, D., Rottman, J.W., Eckermann, S.D., Hulburt, E.O., 2001. A hybrid method for wave propagation from a localized source, with application to mountain waves. Q. J. R. Meteorol. Soc. 127 (571), 129–146. https://doi.org/10.1256/smsqj.57107.

Chan, P.W., 2010. Generation of an Eddy dissipation rate map at the Hong Kong international airport based on doppler lidar data. J. Atmos. Ocean. Technol. 28, 37–49.

Clark, T.L., Peltier, W.R., 1977. On the evolution and stability of finite-amplitude mountain waves. J. Atmos. Sci. 34, 1715–1730.

Díaz-Fernández, J., Quitián-Hernández, L., Bolgiani, P., Santos-Muñoz, D., García-Gago, A., Fernández-González, S., Valero, F., Merino, A., García-Ortega, E., Sánchez, J.L., Sastre, M., Martín, M.L., 2020. Mountain waves analysis in the vicinity of the Madrid-Barajas airport using the WRF model. Adv. Meteorol. 2020 https://doi.org/10.1155/2020/8871546.

Díaz-Fernández, J., Bolgiani, P., Santos-Muñoz, D., Sastre, M., Valero, F., Sebastián-Martín, L.I., Fernández-González, S., López, L., Martín, M.L., 2021. On the characterization of mountain waves and the development of a warning method for aviation safety using WRF forecast. Atmos. Res. 258 https://doi.org/10.1016/j.atmosres.2021.105620.

Díaz-Fernández, J., Bolgiani, P., Santos-Muñoz, D., Quitián-Hernández, L., Sastre, M., Valero, F., Farrán, J.I., González-Alemán, J.J., Martín, M.L., 2022. Comparison of the WRF and HARMONIE models ability for mountain wave warnings. Atmos. Res. 265 https://doi.org/10.1016/j.atmosres.2021.105890.

EASA (European Union Aviation Safety Agency), 2019. Annual Safety Review 2019. https://doi.org/10.2822/098259.

Evans, J.K., 2014. An updated examination of aviation accidents associated with turbulence, wind shear and thunderstorm. In: Technical Report AMA Report Number 14–14. Analytical Mechanics Associates, Inc.

FAA (Federal Aviation Administration), 2016. Advisory Circular 00-6B: Aviation Weather doi:afs-800 ac 91–97.

Fernández-González, S., Sánchez, J.L., Gascón, E., López, L., García-Ortega, E., Merino, A., 2014. Weather features associated with aircraft icing conditions: A case study. Sci. World J. 2014 https://doi.org/10.1155/2014/279063.

Fernández-González, S., Merino Suances, A., Bolgiani, P., 2019. Pronóstico de engelamiento y ondas de montaña mediante modelos mesoescalares orientado a mejorar la seguridad aérea. In: Sexto Simposio Nacional de Predicción "Memorial Antonio Mestre.". https://doi.org/10.31978/639-19-010-0.273.

Frech, M., 2004. A simple method to estimate the eddy dissipation rate from SODAR/RASS measurements. In: In 16th Symposium on Boundary Layers and Turbulence.

Geresdi, I., Rasmussen, R., 2005. Freezing drizzle formation in stably stratified layer clouds. Part II: the role of giant nuclei and aerosol particle size distribution and solubility. J. Atmos. Sci. 62 (7), 2037–2057. https://doi.org/10.1175/JAS3452.1.

Gultepe, I., Sharman, R., Williams, P.D., Zhou, B., Ellrod, G., Minnis, P., Trier, S., Griffin, S., Yum, S.S., Gharabaghi, B., Feltz, W., Temimi, M., Pu, Z., Storer, L.N., Kneringer, P., Weston, M.J., Chuang, H. ya, Thobois, L., Dimri, A.P., Dietz, S.J., França, G.B., Almeida, M.V., Neto, F.L.A., 2019. A review of high impact weather for aviation meteorology. Pure Appl. Geophys. 176, 1869–1921. https://doi.org/10.1007/s00024-019-02168-6.

Hersbach, H., Bell, B., Berrisford, P., Hirahara, S., Horányi, A., Muñoz-Sabater, J., Nicolas, J., Peubey, C., Radu, R., Schepers, D., Simmons, A., Soci, C., Abdalla, S., Abellan, X., Balsamo, G., Bechtold, P., Biavati, G., Bidlot, J., Bonavita, M., De Chiara, G., Dahlgren, P., Dee, D., Diamantakis, M., Dragani, R., Flemming, J., Forbes, R., Fuentes, M., Geer, A., Haimberger, L., Healy, S., Hogan, R.J., Hólm, E., Janisková, M., Keeley, S., Laloyaux, P., Lopez, P., Lupu, C., Radnoti, G., de Rosnay, P., Rozum, I., Vamborg, F., Villaume, S., Thépaut, J.N., 2020. The ERA5 global reanalysis. Q. J. R. Meteorol. Soc. 146 https://doi.org/10.1002/qj.3803.

Hong, S.Y., Noh, Y., Dudhia, J., 2006. A new vertical diffusion package with an explicit treatment of entrainment processes. Mon. Weather Rev. 134 (9) https://doi.org/10.1175/MWR3199.1, 2318–234.

Huang, R., Sun, H., Wu, C., Wang, C., Lu, B., 2019. Estimating eddy dissipation rate with QAR flight big data. Appl. Sci. (Switzerland) 9 (23), 1–14. https://doi.org/10.3390/app9235192.

Ikeda, K., Rasmussen, R.M., Hall, W.D., Thompson, G., 2007. Observations of freezing drizzle in extratropical cyclonic storms during IMPROVE-2. J. Atmos. Sci. 64 (9), 3016–3043.

International Civil Aviation Organization (ICAO), 2001. Meteorological service for international air navigation. In: Annex 3 to the Convention on International Civil Aviation, 14th Ed. ICAO Rep, p. 128.

Kim, J., Chun, H.Y., 2011. Statistics and possible sources of aviation turbulence over South Korea. J. Appl. Meteorol. Climatol. 50, 311–324.

Kramar, V., Kouznetsov, R., 2002. A new concept for estimation of turbulent parameter profiles in the ABL using SODAR data. J. Atmos. Ocean. Technol. 19, 1216–1224.

Kuettner, J., 1939. Zur Entstehung der Fohnwelle. Beitr. Phys. Frei Atmos. 25, 251–299.

Lane, T.P., Doyle, J.D., Sharman, R.D., Shapiro, M.A., Watson, C.D., 2009. Statistics and dynamics of aircraft encounters of turbulence over Greenland. Mon. Weather Rev. 137, 2687–2702.

Lilly, D.K., Kennedy, P.J., 1973. Observations of a Stationary Mountain Wave and its Associated Momentum Flux and Energy Dissipation. J. Atmos. Sci. 30, 1135–1152.

MacCready, P.B., 1964. Standardization of gustiness values from aircraft. J. Appl. Meteorol. 3, 439–449.

NTSB (National Transportation Safety Board), 2014. General Aviation: Identify and Communicate Hazardous Weather. http://www.ntsb.gov/safety/mwl/Pages/mwl7_2014.aspx (accessed 21 September 2021).

Parker, T.J., Lane, T.P., 2013. Trapped mountain waves during a light aircraft accident. Aust. Meteorol. Oceanogr. J 63, 377–389.

Rai, R.K., Berg, L.K., Kosović, B., Mirocha, J.D., Pekour, M.S., Shaw, W.J., 2017. Comparison of measured and numerically simulated turbulence statistics in a convective boundary layer over complex terrain. Bound.-Layer Meteorol. 163 (1), 69–89. https://doi.org/10.1007/s10546-016-0217-y.

Saha, S., Moorthi, S., Pan, H., Wu, X., Wang, J., Nadiga, S., Tripp, P., Kistler, R., Woollen, J., Behringer, D., Liu, H., Stokes, D., Grumbine, R., Gayno, G., Wang, J., Hou, Y., Chuang, H., Juang, H.H., Sela, J., Iredell, M., Treadon, R., Kleist, D., Van Delst, P., Keyser, D., Derber, J., Ek, M., Meng, J., Wei, H., Yang, R., Lord, S., van den Dool, H., Kumar, A., Wang, W., Long, C., Chelliah, M., Xue, Y., Huang, B., Schemm, J., Ebisuzaki, W., Lin, R., Xie, P., Chen, M., Zhou, S., Higgins, W., Zou, C., Liu, Q., Chen, Y., Han, Y., Cucurull, L., Reynolds, R.W., Rutledge, G., Goldberg, M., 2010. NCEP climate forecast system reanalysis (CFSR) 6-hourly products, January 1979 to December 2010, research data archive at the national center for atmospheric research. Comput. Inform. Syst. Lab. doi:10.5065/ D69K487J. (accessed on 15 February 2022).

Sarpkaya, T., Robins, R.E., Delisi, D.P., 2001. Wake-Vortex Eddy-dissipation model predictions compared with observations. J. Aircr. 38, 687–692.

Sharman, R.D., Pearson, J.M., 2017. Prediction of energy dissipation rates for aviation turbulence. Part I: forecasting nonconvective turbulence. J. Appl. Meteorol. Climatol. 56 (2), 317–337.

Sharman, R.D., Tebaldi, C., Wiener, G., Wolff, J., 2006. An integrated approach to mid- and upper-level turbulence forecasting. Wea. Forecast. 21, 268–287.

Sharman, R.D., Trier, S.B., Lane, T.P., Doyle, J.D., 2012. Sources and dynamics of turbulence in the upper troposphere and lower stratosphere: A review. Geophys. Res. Lett. 39 (12).

Sharman, R.D., Cornman, L.B., Meymaris, G., Pearson, J., Farrar, T., 2014. Description and derived climatologies of automated in situ eddy dissipation rate reports of atmospheric turbulence. J. Appl. Meteorol. Climatol. 53, 1416–1432. https://doi.org/10.1175/JAMC-D-13-0329.1.

Shevchenko, O., Lee, H., Snizhko, S., Mayer, H., 2013. Long-term analysis of heat waves in Ukraine. Int. J. Climatol. 34 (5), 1642–1650. DOI: 10.1002/ joc.3792.

Skamarock, W.C., Klemp, J.B., 2008. A time-split nonhydrostatic atmospheric model for weather research and forecasting applications. J. Comput. Phys. 227 (7), 3465–3485. https://doi.org/10.1016/j.jcp.2007.01.037.

Smith, R.B., 1985. On severe downslope winds. J. Atmos. Sci. 42, 2597–2603.

Thompson, G., Field, P.R., Rasmussen, R.M., Hall, W.D., 2008. Explicit forecasts of winter precipitation using an improved bulk microphysics scheme. Part II: Implementation of a new snow parameterization. Mon. Weather Rev. 136 (12), 5095–5115. https://doi.org/10.1175/2008MWR2387.1.

Trier, S.B., Sharman, R., 2016. Mechanisms influencing cirrus banding and aviation turbulence near a convectively enhanced upper-level jet stream. Mon. Weather Rev. 144, 3003–3027. https://doi.org/10.1175/MWR-D-16-0094.1.

Troen, I.B., Mahrt, L., 1986. A simple model of the atmospheric boundary layer; sensitivity to surface evaporation. Bound.-Layer Meteorol. 37 (1), 129–148.

Večenaj, Ž., De Wekker, S.F., Grubišić, V., 2011. Near-surface characteristics of the turbulence structure during a mountain-wave event. J. Appl. Meteorol. Climatol. 50 (5), 1088–1106.

Wyngaard, J.C., 2004. Toward numerical modeling in the “Terra Incognita.”. J. Atmos. Sci. 61 (14), 1816–1826. https://doi.org/10.1175/1520-0469(2004)061<1816:TNMITT>2.0.CO;2.

Zhang, T., Zhao, C., Gong, C., Pu, Z., 2020. Simulation of wind speed based on different driving datasets and parameterization schemes near dunhuang wind farms in Northwest of China. Atmosphere 11 (6), 647.

Zovko-Rajak, D., Lane, T.P., 2014. The generation of near- cloud turbulence in idealized simulations. J. Atmos. Sci. 71, 2430–2451. https://doi.org/10.1175/JAS-D-13-0346.1.